Article

Spectral Analysis, Biocompounds, and Physiological Assessment of Cork Oak Leaves: Unveiling the Interaction with *Phytophthora cinnamomi* and Beyond

Rui Guerra [1,2,*], Rosa Pires [2], António Brázio [2], Ana Margarida Cavaco [2], Gabriela Schütz [2,3] and Ana Cristina Coelho [2,4,*]

1   Departamento de Física, Faculdade de Ciências e Tecnologia, Universidade do Algarve, 8005-139 Faro, Portugal
2   Center for Electronic, Optoelectronic and Telecommunications (CEOT), Universidade do Algarve, 8005-139 Faro, Portugal; rmpires@ualg.pt (R.P.); ambrazio@ualg.pt (A.B.); acavaco@ualg.pt (A.M.C.); gschutz@ualg.pt (G.S.)
3   Instituto Superior de Engenharia, Universidade do Algarve, 8005-139 Faro, Portugal
4   Escola Superior de Educação e Comunicação, Universidade do Algarve, 8005-139 Faro, Portugal
*   Correspondence: rguerra@ualg.pt (R.G.); acoelho@ualg.pt (A.C.C.); Tel.: +351-919073178 (A.C.C.)

Abstract: The cork oak tree (*Quercus suber* L.) symbolizes *the Montado* landscape in Portugal and is a central element in the country's social and economic history. In recent decades, the loss of thousands of cork oaks has been reported, revealing the ongoing decline of these agroforestry ecosystems. This emblematic tree of the Mediterranean Basin is host to the soil-born root pathogen *Phytophthora cinnamomi*, an active cork oak decline driver. In this framework, the early diagnosis of trees infected by the oomycete by non-invasive methods should contribute to the sustainable management of cork oak ecosystems, which motivated this work. Gas exchange and visible/near-infrared (400–1100 nm) reflectance spectroscopy measurements were conducted on leaves of both control and *P. cinnamomi* inoculated plants. These measurements were taken at 63, 78, 91, 126, and 248 days after inoculation. Additionally, at the end of the experiment, biochemical assays of pigments, sugars, and starch were performed. The spectroscopic measurements proved effective in distinguishing between control and inoculated plants, while the standard gas exchange and biochemistry data did not exhibit clear differences between the groups. The spectral data were examined both daily and globally, utilizing the PARAFAC method applied to a three-way array of samples × wavelengths × days. The separation of the two plant groups was attributed to variations in water content ($4v\,(O-H)$); shifts in the spectra red edge; and structural modifications in the epidermal layer and leaves' mesophyll. These spectral signatures can assist in the field identification of cork oaks that are interacting with *P. cinnamomi*.

Keywords: cork oak decline; *Quercus suber-Phytophthora cinnamomi* interaction; reflectance spectra; disease spectral monitoring

1. Introduction

In Portugal, the cork oak (*Quercus suber* L.) is part of the native evergreen forests. These are known as *montados*, *cork oak forests* and *holm oak forests*. They cover a vast area of 1 million hectares on the mainland, representing a third of the country's forested territory [1]. The canopy cover of cork and holm oak forests was monitored between 1990 and 2015, showing a trend towards forest degradation [2]. Bento et al. [3] emphasize that determining the percentage of forest cover is important for assessing their sensitivity to drought, highlighting the vulnerability of forests located in central, SW and NE Portugal. These reports are consistent with the deteriorating trend documented over the last few decades, threatening the survival of these highly productive agroforestry systems, which are critical to the Iberian Peninsula's rural economy [4,5]. In the Mediterranean woodlands,

the oomycete *Phytophthora cinnamomi* infects the roots of oaks [6] and shrubs [7,8]. The abundance of the parasite contributes to tree death along with other factors [9]. Its abundance and spread is driven by climatic variations [10]. The ecological dynamics of the oomycete are adapted to variations in temperature and humidity across seasons, and their abundance and spread originate from recognized disease foci and through the sporadic transmission of disease over longer distances [11].

The degradation trend observed in cork and holm oak forests in Portugal raises concerns about the survival of these essential agroforestry systems. In the context of Mediterranean woodlands, where the oomycete *P. cinnamomi* poses a threat to tree mortality, remote sensing using visible and infrared imaging has become a valuable tool for monitoring vegetation health and detecting crop diseases by quantifying spectral reflectance changes [4,10].

The significance of remote sensing for Earth's surface has grown considerably since the introduction of early weather satellites like Landsat and Nimbus. These satellites have revolutionized the observation of forest and crop canopies through the utilization of visible and infrared imaging, enabling the analysis of light reflection, absorption, and transmission by plant leaves. The technique has been widely used in agriculture to monitor crop growth, nutrient status, and stress responses [12]. In their comprehensive survey, Ustin and Jacquemoud [13] delve into the intricate relationship between leaf structure, biochemistry, and the optical properties of plants. Within the visible to near-infrared band (400–1100 nm), the spectral reflectance characteristics primarily rely on the absorption of chlorophyll in the blue and red regions, as well as the absorption bands of water in the infrared [13,14]. Moreover, reflectance plateaus in the infrared region are associated with cellular structure, leading to higher reflectivity values compared to the lower reflectivity in the visible range caused by pigment absorption [15]. These differences in reflectance between the visible and infrared spectra serve as indicators of vegetation health and condition, particularly at the red edge transition occurring between 680 and 740 nm [16]. Indeed, many applications for crop disease detection rely on quantifying changes in these characteristics [17].

In the context of plant disease monitoring, visible-near infrared (Vis/NIR) spectroscopy serves as a valuable tool. While both remote sensing and Vis/NIR spectroscopy rely on the fundamental principle of reflectance, there are notable differences between the two approaches. Vis/NIR spectroscopy is typically performed under controlled conditions or by directly contacting the leaf, whereas remote sensing captures spectra or multi-spectral images from an airborne platform.

Thus, Vis/NIR spectroscopy acts as a testing ground for remote sensing, enabling measurements in controlled conditions and facilitating the examination of the correlation between spectral bands and vegetation traits, either structural or related to pathologies. It can also be employed as a standalone technique for proximal or contact measurements.

For instance, Slaton et al. [14] conducted a study to explore the relationship between near-infrared reflectance (NIRR) at 800 nm and leaf structural characteristics in alpine angiosperms. They discovered a strong correlation between NIRR and leaf bicoloration, leaf cuticle thickness, and the exposed mesophyll cell surface area per unit leaf surface area. This finding established a clear link between reflectance and plant structure and function. In the same line of research, Buitrago et al. [18] estimated leaf traits from infrared measurements (1.4–16.0 μm, outside the visible-near infrared range used in this work) taken from various plant species and partial least squares regression models. Results showed that leaf thickness, water content, cellulose, lignin, and stomata density could be estimated with moderate to good accuracy.

The changes induced in the spectra by the presence of pathogens are surprisingly fast. This has been shown in the investigation by Kuska et al. [19], which used a microscope with a hyperspectral camera to analyze the interactions between *Blumeria graminis* f. sp. *hordei* and barley genotypes with different susceptibility levels. Changes in hyperspectral signatures, particularly in the green and red range, were observed within 48 h after inocula-

tion. Specific reflectance patterns indicated resistance, and hyperspectral imaging allowed for early detection of hypersensitive response (HR) spots.

A correlation between the emergence of infections and concurrent alterations in spectral reflectance seems evident. Numerous researchers have extensively utilized this relationship, typically employing various statistical multivariate analyses on spectral data to differentiate between healthy and infected plants or even among different types of plant diseases. The primary goal of these investigations is to enable the early detection of diseases (prior to visible symptoms) and/or their widespread occurrence through remote sensing. This approach has been applied to virtually all major disease categories [20]. For instance, it has been employed to identify infestations such as soybean cyst nematodes [21], aphids in winter wheat [22], and mealybugs in tomato plants [23]. Furthermore, it has been utilized to diagnose fungal diseases like sudden death syndrome [21], yellow rust and powdery mildew in winter wheat [22], target spots in tomato [24], and laurel wilt [25]. Additionally, bacterial diseases such as bacterial spots in tomato [24] and viral infections like Huanglongbing in citrus [26] have also been investigated using this approach.

Detecting *Phytophthora cinnamomi* early and accurately in cork oak is crucial for effective management of decline. However, traditional methods for oomycete detection involve time-consuming laboratory analyses and can be costly. Therefore, it is particularly relevant to consider the investigations conducted on *Phytophthora infestans*, such as those related to tomato late blight [24], for the present study. Newby et al. [27] monitored the effects of *P. cinnamomi* infection in Australian native vegetation through a two-factor experiment involving infection and water stress. They observed contrasting spectral responses between the inoculated and water stress groups. Hardoim et al. [28] utilized Fourier Transform Infrared Spectroscopy and found that metabolic patterns in cork oak roots were altered as early as 2 h post-inoculation (hpi). Aubard et al. [5] assessed the decline of oak stands in Portugal and developed an effective monitoring tool for forest health and productivity using the NDVI (Normalized Difference Vegetation Index). They successfully correlated long-term trends in NDVI productivity. Another aspect explored in this study is the analysis of spectral characteristics over time following pathogen inoculation. This approach was also applied by Afonso et al. [29] in their research on citrus trees infected with Citrus Tristeza Virus. They found that discrimination between control and infected groups was not possible on certain measurement days, but became evident when analyzing the temporal trend.

The cork industry and the implementation of efficient disease management strategies would greatly benefit from the development of non-destructive and rapid methods for detecting oomycete-infected plants. In this study, we investigated the feasibility of utilizing VIS/NIR reflectance spectroscopy on cork oak leaves to identify plants that have been inoculated with *P. cinnamomi* and are engaged in an interaction with the oomycete. To achieve this, we employed chemometric techniques to establish classification models for the cork oak-*P. cinnamomi* interaction. Spectrum data were collected from leaves of both inoculated and non-inoculated cork oak plants to support our analysis.

2. Materials and Methods

The methodological design defined for this project is outlined in Figure 1. The scheme presents the different experimental approaches followed, which included the spectroscopic acquisition and the measurement and quantification of physiological and biochemical parameters in non-inoculated cork oak plants and in cork oak plants inoculated with *P. cinnamomi* over a period of 248 days.
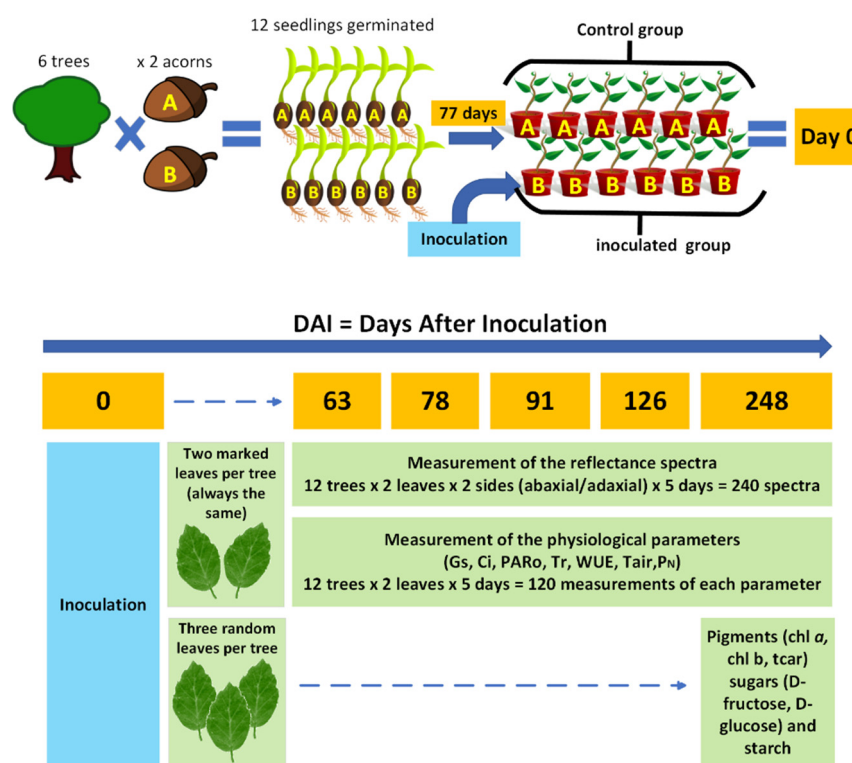
Figure 1. Representative scheme of the project's methodological design. (Control group: six non-inoculated cork oak plants and control plants, times two acorns, A and B; Inoculated group: six cork oak plants inoculated with *P. cinnamomi*; chl-*a*: chlorophyll-a; chl-*b*: chlorophyll-b; t*car*: total carotenoids; *gs*: stomatal conductance; Ci: intercellular CO_2 concentration; Tr: transpiration rate; WUE: water-use efficiency; Tair: air temperature; PARo: external photosynthetically active radiation; and P_N: net photosynthetic rate).

2.1. Biological Material

The sample originated from twelve seedlings germinated from acorns with provenance in six cork oak trees. These parental cork oak trees were from Cachopo in the Algarve region (Portugal) and showed signs of decline. After germination, seventy-seven-day-old cork oak plants were divided into two groups of six plants each. One group was kept as the control, and the plants in the second group were inoculated with PA 45 *Phytophthora cinnamomi* isolate. Both groups, control and inoculated, had one plant that germinated from seeds of the same mother tree (as illustrated in Figure 1 through the A and B acorn groups).

Briefly, for the preparation of control and inoculated plants, twelve 77-day-old cork oak plants were removed from the germination alveoli, the organic substrate was removed, and the plant roots were kept in contact with moistened absorbent paper. For the inoculation, a 2 cm^2 agar plug of *P. cinnamomi* mycelium isolate PA45, grown in clarified V8 (Campbell Soup) semi-solid agar in the dark at 25 °C for 9 days, was placed mycelial-surface-down on the taproot of 6 cork oak plants—inoculated plants. A second group of 6 plants was not in contact with the oomycete—non-inoculated plants. The roots of the inoculated and non-inoculated plants were covered with aluminum foil and kept on the moistened trays at 25 °C for 48 h.

Forty-eight hours after inoculation with *P. cinnamomi*, all plants were potted in free-draining plastic pots with a mixture of potting soil (PFLANZ-ERDE) and sand (2/3 for 1/3), transferred outside and watered regularly to container capacity. The assay was run for 248 days under environmental conditions. Since this same set of plants had already been analyzed in a study dedicated to the leaf proteome, further information can be found in the work of Coelho et al. [30].

2.2. Leaf Optical Properties Measurements

To gain insight into the changes occurring at the physiological level of cork oak plants inoculated with *P. cinnamomi*, the reflectance spectra of leaves from 6 control and 6 inoculated cork oak plants were captured twice a week for 6 months and compared. Visible-near infrared (345–1037 nm) spectral data were registered through a portable setup consisting of lamp LS-1-LL (Ocean Optics, Orlando, FL, USA), spectrometer (USB4000, Ocean Optics, USA), and bifurcated fiber optic with leaf clip for reflectance measurements (PP Systems, Amesbury, MA, USA). Spectral acquisitions were performed at five time intervals (63, 78, 91, 126, and 248 days after inoculation (DAI) with *P. cinnamomi*), capturing data from both the abaxial and adaxial faces of the leaves (two leaves per plant), thereby providing an evaluation of the phenomenon under study over a comprehensive timespan (248 days), with all plants measured on each day, approximately at the same time of the day (14 h) and in sequence. Statistical analyses were conducted using Matlab R2019a (MathWorks, Natick, MA, USA) and the PLS Toolbox for Matlab [31]. The Wilcoxon Rank Sum Test was applied using the ranksum function in Matlab. Additionally, the PLS Toolbox provided the necessary functions for Multiplicative Scatter Correction (mscorr), Savitzky–Golay filtering (savgol), and PARAFAC analysis (parafac).

2.3. Calculation of the Vegetative Indices

From the spectral data, the vegetative indices were calculated according to the formulas presented in Table 1.

Table 1. Vegetation Indices (VI) used in this work.

Name	Formula *	Reference
NDVI	$(N - R)/(N + R)$	[32]
GNDVI	$(G - R)/(G + R)$	[33]
WBI	R_{950}/R_{900}	[34]
SAVI	$[(1 + L)(N - R)]/(N + R + L), L = 0.5$	[35]
O1	$N - aR, a = 1$	[36]
O2	R/N	[37]
O3	G/R	[38]
O4	N/R	[39]
PRI	$(R_{531} - R_{570})/(R_{531} + R_{570})$	[40]
RSVI	$(R_{714} + R_{752})/2 - R_{733}$	[41]
MCARI	$[(R_{700} - R_{670}) - 0.2(R_{700} - R_{500})] \times R_{700}/R_{670}$	[42]
VARI	$(G - R)/(G + R - B)$	[35]
WI	R_{900}/R_{970}	[34]
BRI	$(1/R_{550} - 1/R_{700})/N$	[43]

* The symbols R, G, B, and N correspond to the red, green, blue, and near-infrared bands, respectively, and were calculated based on the average values of the respective wavelength ranges (600–700 nm for red, 500–600 nm for green, 400–500 nm for blue, and 800–900 nm for near-infrared). Additionally, Rxyz represents the monochromatic reflection at a wavelength of xyz nm. The explanations of the acronyms in the first column can be found in the main text. The references providing a more detailed introduction or explanation of the VIs are listed in the third column.

Relatively to the contents of Table 1, the Normalized Difference Vegetation Index (NDVI) is the most widely adopted VI to determine the greenness (health) of vegetation [32]. NDVI values range from 1 to −1. Healthy NDVI values are greater than 0.3, and lower NDVI values represent barren or drought-tolerant plants. The Green Normalized Difference Vegetation Index (GNDVI) method is used to estimate photosynthetic activity and is a commonly used vegetation index to determine water and nitrogen uptake into the plant

canopy [33]. The Water Index (WI) is sensitive to changes in canopy water status. As the water content of vegetation canopies increases, the strength of the absorption around 970 nm increases relative to that at 900 nm [34]. We included a similar index, calculated from the reflectance around 950 nm instead. This is called the Water Band Index (WBI). The soil-adjusted vegetation index (SAVI) accounts for the differential red and near-infrared extinction through the vegetation canopy. The index is a transformation technique that minimizes soil brightness influences from spectral vegetation indices involving red and NIR wavelengths [35]. The indices O1–O4 are simple ratios and/or differences between two bands less used in the literature and that do not have a uniformly adopted nomenclature. O1 is a simple version of the Weighted Difference Vegetation Index (WDVI) [36] with a coefficient taken as 1. Since it measures the difference in height between the red and NIR plateaus, and the latter depends on the scattering by the leaf structure, it may be related to changes in leaf structure. O2 is the simple red/NIR ratio [37], while O4 is simply its inverse and is usually called the simple ratio NIR/RED Difference Vegetation Index (DVI). Finally, O3 is the green/red ratio [38]. The Photochemical Reflectance Index (PRI) is sensitive to changes in carotenoid pigments (e.g., xanthophyll pigments) in live foliage [40]. The Red Edge Vegetation Stress Index (RVSI) identifies spectral changes in the red edge, which may also be traced to changes in leaf structure [41]. The Modified Chlorophyll Absorption in Reflectance Index (MCARI) minimizes the effects of nonphotosynthetic materials on spectral estimates of absorbed photosynthetically active radiation [42]. The Visible Atmospherically Resistant Index (VARI) is designed to emphasize vegetation in the visible portion of the spectrum while mitigating illumination differences and atmospheric effects [35]. The Browning Reflectance Index (BRI) was for the estimation of superficial scald development in anthocyanin-free fruit upon a background of Chl and Car absorption [43], but we included it in the attempt to find browning in the leaves.

2.4. Leaf Gas Exchange Measurements

Net photosynthetic rate (P_N) (μmol CO_2 m^{-2}s^{-1}), transpiration rate (Tr) (mmol H_2O m^{-2}s^{-1}), stomatal conductance (g_s) (mol H_2O m^{-2}s^{-1}), intercellular CO_2 concentration (C_i) (μmol CO_2 mol^{-1}), and water-use efficiency (WUE) were determined for the two leaves per plant used in the spectroscopy assays taken at 63, 78, 91, 126, and 248 days after inoculation (DAI), with an infrared gas analyzer (IRGA) (LI-6400 Portable Photosynthesis System, LI-COR, Lincoln, NE, USA) equipped with a 2 × 3 cm clear-bottom chamber (reference 6400-08, LI-COR, Lincoln, NE, USA). The measurements were performed at the aforementioned five time intervals outdoors, under environmental conditions. To comply with the circadian rhythm of photosynthesis and gas exchange, which can affect both gas exchange and spectra, the measurements were always performed in the time interval of 10–13 h, during which the IRGA measurements were taken before the spectroscopy measurements. The IRGA measurements were always taken in the morning, and the spectroscopy measurements were taken in early afternoon. In either case, the acquisitions were performed during the period when photosynthetic processes were at a stable and maximum level.

2.5. Quantification of Biochemical Parameters

At the end of the assay, the leaves of cork oak plants, inoculated and control, were collected, immediately frozen in liquid nitrogen, and stored at −80 °C until further use for quantification of biochemical parameters. Three random leaves per plant (N = 12) were retrieved for the quantitative determination of leaf pigments and sugars. Pigment quantification was performed by UV/VIS spectroscopy expressed in mass (mg) per unit area (m^2). The leaf material was submersed in 5 mL of methanol (pure solvent) for 48 h in the dark at 4 °C. Two aliquots were taken from each of the samples (2 technical replicates) and assayed in a spectrophotometer (model UV-160 A, Shimadzu Corporation, Kyoto, Japan). The content of chlorophyll-a (Chl *a*), chlorophyll-b (Chl *b*), total chlorophyll (Chl *a* + *b*), and

total carotenoids (t*car*) were calculated according to the equations of Lichtenthaler [44,45]. Additionally, the Chl *a/b* ratio and Chl *a* + *b*/t*car* ratio were calculated.

For the quantitative determination of sugars, the whole extract of soluble sugars was obtained by submerging the cork oak leaf discs (100–200 mg fresh weight) in 1 mL ethanol 80%, followed by incubation at 80 °C for 15 min.

This procedure was repeated 2 times, and then an aliquot of activated charcoal was added to 200 μL extract and centrifuged at 13,000 rpm for 1–2 min. Quantification was performed on the supernatant. The solid phase (plant leaves) was kept in the original Eppendorf tube and stored at −20 °C for later use. The determination of leaf starch content was carried out using the hydrolysis of the starch and the subsequent quantification of the obtained glucose equivalents. Cork oak leaves were ground in a mortar and pestle with quartz sand and distilled water (1 mL), and the resulting mixture was centrifuged at 15,000 rpm for 2 min; the supernatant was discarded, and the pellet was re-suspended in water (1 mL). Prior centrifugation and resuspension procedures were repeated three times. Then, the re-suspended pellet was autoclaved for 20 min at 100 °C. After cooling, one hundred microliters of the resulting starch suspension were submitted to enzymatic hydrolysis by the addition of 0.5 mL of amyloglucosidase (1.4 U) and α-amylase (2U) solution and incubation overnight at 37 °C. After centrifugation of the hydrolysis solution at 15,000 rpm for 1 min, the resulting glucose present in the supernatant was used for the quantification of the leaf starch content. Both the soluble sugars and the resulting glucose from starch cleavage samples were assayed enzymatically with the K-SUFRG–Sucrose/D-Fructose/D-Glucose Assay Kit (Megazyme International, Ireland) at 340 nm following the supplier's instructions, on a Bio Tek Synergie 4 Plate Reader (BioTek Instruments, Inc., Santa Clara, CA, USA). Each sample was analyzed in triplicate.

3. Results and Discussion

3.1. Global Remarks on the Spectra Acquisition and Preprocessing

- Signal-to-noise ratio

Since the aim of the spectral measurements was to detect potential variations between the control and inoculated plant groups, it is crucial to ensure that the spectra exhibit a suitable signal-to-noise ratio (SNR) across the entire range. Given that these differences might be subtle, it is essential to assess the SNR for each wavelength. SNR is computed by dividing the average signal by its standard deviation, obtained from a series of measurements. In a previous study, the same spectrometer was employed for non-invasive prediction of the internal quality of 'Jintao' kiwifruit [29]. It was determined that the spectral ranges suitable for calibration exhibited an SNR greater than 200. Following a similar procedure, the SNR was calculated in this study, and the range from 530 to 920 nm was determined to be the optimal one. Beyond this range, the SNR curve rapidly declines, which can be attributed to two factors: (i) the spectral response of the spectrometer's detector and (ii) the absorption caused by the pigments present in the leaves. For instance, in the range of 400 to 500 nm, both the low spectral response and the significant absorption by chlorophyll and carotenoids contribute to decreased SNR. The absorption by these pigments substantially reduces the reflected signal, leading to lower SNR values. Similarly, the drop observed above 900 nm is associated with the low quantum efficiency of silicon (which falls below 10% beyond 1000 nm) and the absorption caused by water around 960–980 nm. There were no significant differences between the SNR curves calculated from the adaxial and abaxial sides, as well as between inoculated and control leaves.

- Experimental motivation for the choice of preprocessing

The spectral acquisition was conducted under sunlight and challenging conditions for the equipment. For instance, on hot days, the cooling of the light source was less effective, leading to gradual fluctuations in light intensity. Similarly, the spectrometer's response and dark noise counts exhibited slow drifts over time. Consequently, using absolute reflectance values for comparing the two groups is not recommended. Instead,

a preprocessing technique is necessary to mitigate the additive and multiplicative effects induced by environmental changes. Therefore, the spectra underwent Multiplicative Scatter Correction (MSC) as a preprocessing step. MSC was calculated from the average of the spectra from all days and all plants (i.e., including both groups). Prior to applying MSC, the spectral data were limited to the range of 530–920 nm, as determined by the SNR analysis. It is important to note that MSC causes a loss of direct interpretability for the absolute values of reflectance. However, the overall shape of the spectrum is preserved, allowing for the identification of local variations within specific spectral wavebands through changes in the spectrum shape and its relation to other bands. Figure 2 displays the superimposed spectra after applying MSC. The inoculated samples are shown in red, while the control samples are depicted in green. Figure 2A illustrates the reflectance on the abaxial side of the leaves, Figure 2B represents the reflectance on the adaxial side, and Figure 2C displays the average of the four datasets presented in the top figures.
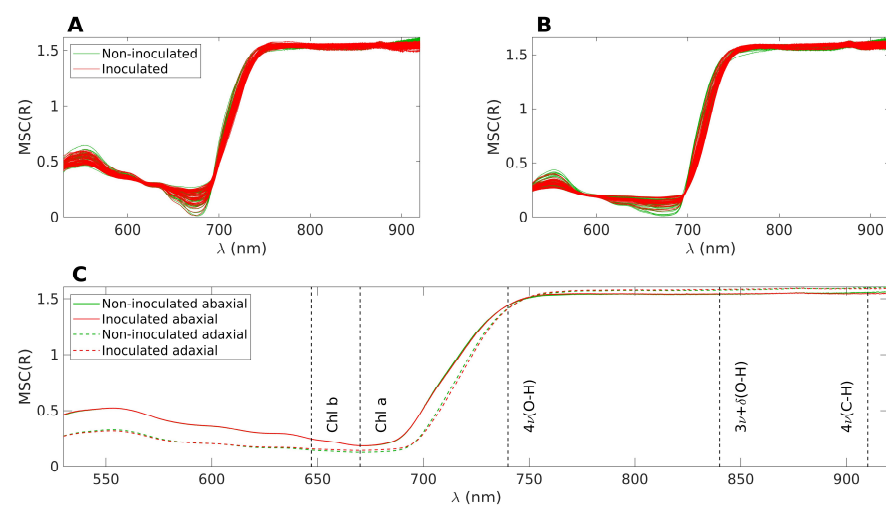

Figure 2. (**A**): Superposition of all MSC treated spectra, abaxial side. The inoculated samples are represented in red and the control samples in green. (**B**): Same as A, but for the adaxial side. (**C**): Average of the four datasets represented in (**A**,**B**). The nominal positions of the main absorption bands are marked with dashed lines.

In Figure 2C, distinct reflectance patterns are observed for the abaxial and adaxial sides. However, when considering the average spectra, it becomes challenging to differentiate between the control and inoculated groups. For the purpose of the following discussion, the spectra can be divided into three main bands. The first band corresponds to the visible range, spanning from 400 to 700 nm, which is influenced by the presence of pigments such as chlorophyll and carotenoids. The second band encompasses the near-infrared (NIR) range, ranging from 750 to 1000 nm, characterized by a plateau. The height of this plateau is primarily determined by the leaf structure, specifically the epidermal layers and the mesophyll [46]. Finally, there is a transition zone between the visible and NIR ranges, often referred to as the red edge. This region exhibits a sharp slope, connecting the low reflectance values in the visible range to higher reflectance levels in the NIR.

The observed phenomenon where the abaxial side reflects more in the visible range and slightly less in the NIR range compared to the adaxial side can be attributed to the optical characteristics of leaf tissues, which have naturally evolved to optimize their interaction with light from above. This optical engineering of the leaf tissues ensures that light is effectively channeled to the chloroplasts for optimal absorption. The palisade parenchyma, with its channel-like structure, plays a key role in facilitating the conduction of light to the chloroplasts. In contrast, the spongy parenchyma, located beneath the palisade parenchyma, induces light scattering, which is particularly important for protecting the leaf from excessive infrared heating. However, when light is incident from below, the order of interaction with the two parenchyma layers is reversed. As a result, the optimal conduction

of light to the chloroplasts is compromised, leading to lower absorption in the visible range and, consequently, higher reflection values. Additionally, the reflection of NIR light is also less efficient on the abaxial side, possibly due to the abaxial epidermis being less reflective than the adaxial epidermis.

Although the overall comparison of spectra collected across all measurement days does not reveal distinct differences between the control and inoculated groups, conducting a specific analysis for each measurement day uncovers noticeable distinctions. These differences were verified using the Wilcoxon Rank Sum Test (also known as the Mann–Whitney U-test), which assesses whether the data in the control and inoculated groups originate from continuous distributions with equal medians. The test is performed for each wavelength individually. The application of the classical t-test across the entire spectral range was not feasible due to a significant portion of wavelengths not meeting the assumptions of normality and homogeneity of variances. Surprisingly, even with these violated assumptions, running the t-test produced results that were highly similar to those obtained with the nonparametric test.

Figure 3 shows the p-values resulting from the Wilcoxon Rank Sum Test, which compares the MSC reflectances of the control and inoculated groups for each measurement day and wavelength. The blue curves represent the p-values obtained for each wavelength, and the pink areas highlight the spectral regions with $p < 0.05$, i.e., those where the data from the two groups are different. In this 5×2 plot, each one of the five rows corresponds to one of the measurement days (63, 78, 91, 126, and 248 DAI), while the two columns represent the abaxial and adaxial sides, respectively.
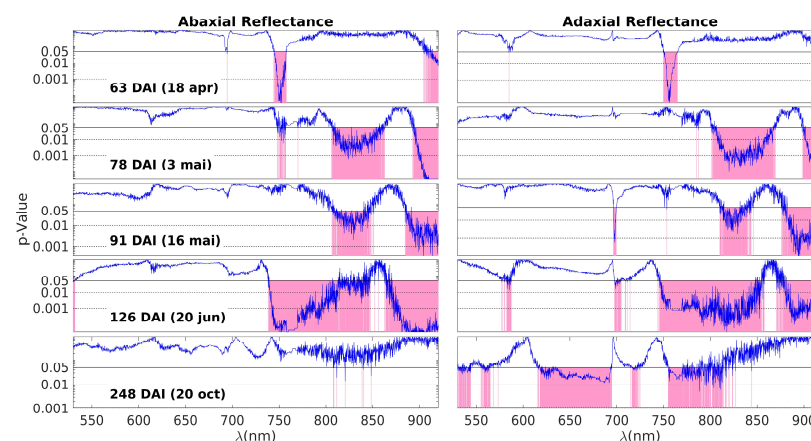

Figure 3. The p-values obtained by the Wilcoxon Rank Sum Test on the comparison between the MSC reflectances of control and inoculated groups from the data obtained on each measurement day (blue lines). Each subplot row corresponds to one of these days (63, 78, 91, 126, and 248 DAI); the left and right columns correspond to the abaxial and adaxial sides, respectively. The p-values are shown as a function of the wavelength. The horizontal lines are at $p = 0.05$ (95% CL) and at $p = 0.01$ (99% CL). Note that the scale is logarithmic. The spectral ranges with a p-value below the threshold of 0.05 are highlighted in pink, meaning that control and inoculated groups have different MSC reflectance medians.

The next plot aims to provide a detailed examination of the spectral data responsible for generating the p-value curves observed in Figure 3. These data are presented in Figure 4, where the control spectra are depicted in green and the inoculated spectra in red. The grey bands highlight the same spectral ranges in which differences between the two groups were observed, also shown in Figure 3. It is important to note that the data were standardized at each wavelength, involving the normalization of each value by subtracting the average and dividing by the standard deviation. This standardization process is essential to facilitate an appropriate visualization of the observed differences.
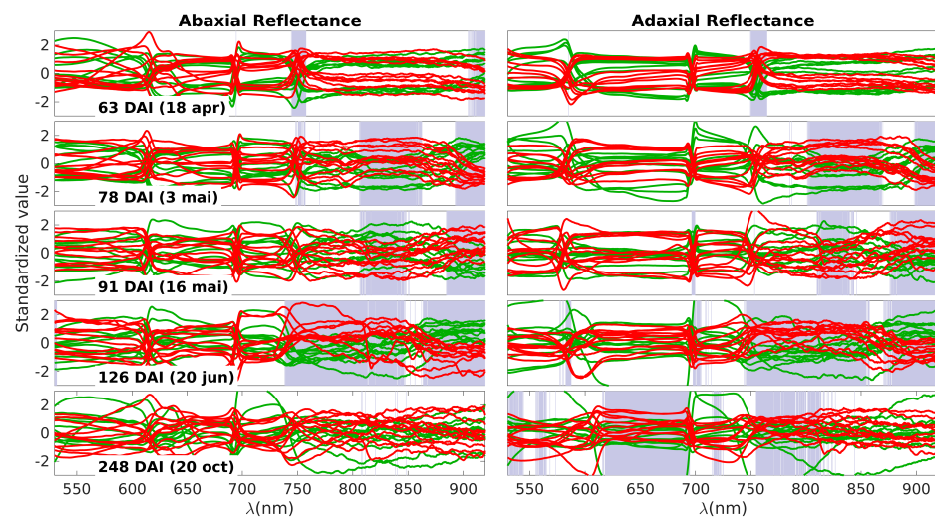
Figure 4. Standardized spectra obtained on each measurement day. Green lines represent the control group and the red lines the inoculated group. Each subplot row corresponds to one of these days (63, 78, 91, 126, and 248 DAI); the left and right columns correspond to the abaxial and adaxial sides, respectively. The grey bands highlight the specific spectral ranges in which differences between the two groups were observed.

On the first day of measurement (63 DAI), there is a noticeable difference primarily around 750 nm. This difference can be attributed to variations in water content (third overtone of the O–H stretching vibration, $4v$ $(O-H)$, and/or a shift in the red edge. The red edge is a sensitive region characterized by a steep slope, marking the transition from low reflectance in the visible range to high reflectance in the NIR plateau. Any alteration in pigments or the leaf structure that affects NIR scattering can lead to changes in the slope of the red edge, making it particularly useful for detecting NIR variations. There is an additional region marked in red on the abaxial side above 900 nm. This can also be influenced by changes in the off-range water absorption peak at 960 nm, corresponding to the second stretching vibration overtone band, $3v$ $(O-H)$. In summary, the most plausible explanation for the differences observed on the first day is as follows: There are initial changes occurring in water levels (indicated by the variations above 900 nm), which slightly impact the NIR plateau. This change is further amplified in the slope of the red edge, making it appear as the primary source of differentiation between the control and inoculated groups.

The patterns observed on days 78, 91, and 126 DAI exhibit patterns that align with variations in water content, reflecting distinctions in the $3v + \delta$ $(O-H)$ combination band and the $3v$ $(O-H)$ combination band at 840 nm and 960 nm, respectively. Additionally, the $4v$ $(C-H)$ band within the 910–930 nm range may contribute to these observations, although distinguishing the individual contributions of these bands can be challenging.

By the fourth day (126 DAI), differences attributable to water remain, but the distinctions across the near-infrared (NIR) plateau become more pronounced. With the exception of a band centered around 870 nm, all regions within the NIR plateau exhibit variations between healthy and inoculated plants. This suggests a significant disruption in the physical structure of the leaves. As previously mentioned, the palisade and spongy parenchyma tissues play a crucial role in light scattering within the NIR plateau. The observed differences across the entire spectral range of the plateau may indicate alterations in the structure of the parenchyma tissues, likely stemming from disparities in the initial water content. Additionally, Figure 4 shows that there is an oscillation in the spectral behavior of these bands. For example, the inoculated group shows higher values in the NIR plateau on the 78 and 126 DAI, but lower on 91 DAI. This may be the result of a more complex and dynamic picture of internal adjustments to the water stress.

The final day of observation reveals a reversal of the observed patterns. On the abaxial side of the leaves, no notable differences are present except for occasional spikes of noise. On the adaxial side, most of the differences within the NIR plateau diminish, with the exception of the band ranging from 750 nm to 820 nm. However, a new development arises in the range of pigments, specifically between 620 nm and 700 nm, where differences between the two groups are apparent. The similarity observed in the NIR plateau between the inoculated and control plants could stem from two possible causes:

(i) The inoculated plants have regained their initial structural integrity;
(ii) The control plants have also experienced structural change.

The latter scenario is plausible, considering that a summer season elapsed between the fourth and final measurements. On the other hand, the differences observed in the pigment range may also be attributed to two potential factors:

(i) Variations in pigment content between the two groups;
(ii) Structural changes in leaf anatomy altering the light path to and from the chloroplasts, thereby impacting reflectance levels.

In the latter hypothesis, the pigment content may be similar in both groups, but the reflectance levels differ. An important clue for discerning which scenario occurred lies in the absence of visible range differences on the abaxial side. This suggests that the pigment content remains unchanged, as any divergence would affect abaxial reflectance. Therefore, the most plausible explanation for the observations on the final day points to structural changes. The leaf structure of the control plants underwent alterations that made their NIR response resemble that of the infected plants. However, these same structural modifications resulted in visible reflectance differences between the two groups. How is this possible?

To comprehend why structural changes can lead to distinct alterations in visible and NIR reflectance patterns, it is important to recall that visible light primarily interacts with the upper portion of the leaf, including the chloroplasts, and extends down to the palisade mesophyll. Conversely, NIR light primarily interacts with the spongy mesophyll, where it is scattered. Based on the observations from the final day, the following conclusions can be drawn:

1. The pigments' content is similar in both the control and inoculated groups;
2. The spongy mesophyll of the control group underwent alterations during the summer and acquired a structure similar to that of the inoculated group;
3. The upper epidermal layer and/or the palisade mesophyll experienced differential changes between the control and inoculated groups, resulting in distinct responses in the visible range.

These findings suggest that while the pigments' content remains consistent, structural modifications in the spongy mesophyll account for the similarity in NIR reflectance between the two groups. Conversely, differential changes in the upper epidermal layer and/or the palisade mesophyll contribute to the divergent responses observed in the visible range. Indeed, the explanation provided aligns with the observed similarity in abaxial reflectances as well. In this scenario, where reflected light predominantly interacts with the spongy mesophyll, the comparable structure of this mesophyll layer in both the control and inoculated groups explains the absence of discernible differences in abaxial reflectances.

- Vegetation Indices

Vegetation Indices (VI) are commonly employed to assess vegetation health through remote sensing. Therefore, it is important to explore whether VI can effectively detect distinctions between the two groups. The indices considered in this study are presented in Table 1, and the results of the discrimination between the inoculated and control groups are shown in Table 2.

Table 2. Results of the discrimination between the inoculated and control groups through the Vegetation Indices used in this work.

Name	% Detection *
NDVI	10
GNDVI	20
WBI	80
SAVI	40
O1	70
O2	10
O3	20
O4	10
PRI	20
RSVI	40
MCARI	10
VARI	30
WI	100
BRI	30

* This is the success rate in detecting differences among the groups, expressed as a percentage. A 100% success rate corresponds to 10 successful detections (5 days × 2 sides, i.e., abaxial and adaxial), which can be easily understood by referring to Figure 5.
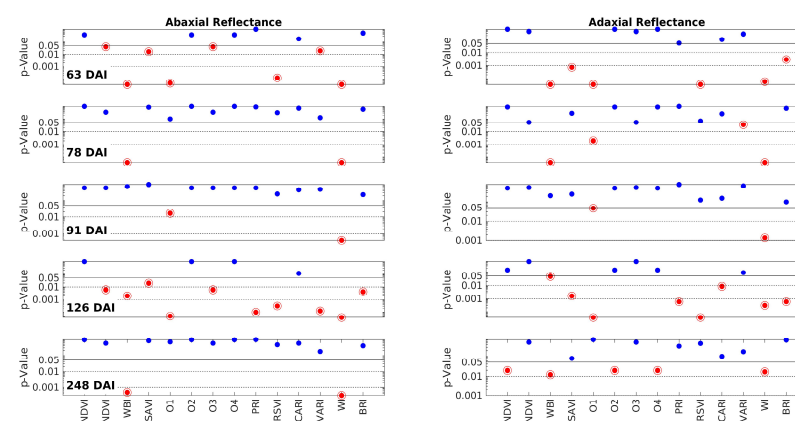

Figure 5. The *p*-values obtained by the Wilcoxon Rank Sum Test on the comparison between the Vegetation Indices (VI) of control and inoculated groups from the data obtained on each measurement day. Each row corresponds to one of these days (63, 78, 91, 126, and 248 DAI); the left and right columns correspond to the abaxial and adaxial sides, respectively. The *p*-values are shown as a function of the wavelength. The horizontal lines are at $p = 0.05$ (95% CL), at $p = 0.01$ (99% CL), and at $p = 0.001$ (99.9% CL). Note that the scale is logarithmic. The points below the threshold $p = 0.05$ are represented in encircled red points, meaning that control and inoculated groups have different medians for that specific VI.

It is crucial to note that the vegetation indices (VI) were derived from the raw reflectance data rather than the MSC-transformed data. Calculating the VIs directly from the raw data ensures that they are not distorted. This approach poses no issue since any potential spectrum fluctuations, which necessitated the application of MSC as a compensation transformation, are naturally accounted for by the nature of the VIs themselves. VIs are primarily defined by ratios, enabling them to compensate for such fluctuations. Figure 5 is analogous to Figure 3, but it focuses on the VIs. Each row in the figure corresponds to one of the measurement days (63, 78, 91, 126, and 248 DAI), while the columns represent the

abaxial and adaxial sides. The p-values are plotted against the VIs, which are shown along the x-axis of the bottom row. The interpretation of the horizontal lines and color codes remains consistent with Figure 3. Furthermore, *p*-values below 0.05 are indicated by a red point encircled by a circumference.

The distribution of the red points in Figure 5 does not exhibit an obvious pattern. It does not align precisely with the distribution of the red–pink ranges in Figure 3. This discrepancy arises because the vegetation indices (VIs) convey nonlinear information that may not directly mirror the spectral information. However, a closer analysis reveals that the two figures point to the same conclusions. As indicated in Table 2, the VIs that are most successful in discriminating between the two groups are WI (100%) and WBI (80%), both of which are associated with water content. The third most successful parameter is O1 or WDVI, which relates to changes in leaf structure. The success rates of all the other VIs are below 50%. Notably, SAVI and RSVI can achieve a 40% success rate. While SAVI is a modified version of NDVI, RSVI targets the red edge, which, as mentioned earlier, may also be influenced by structural changes. In conclusion, the analysis of the VIs confirms the findings of the spectral analysis, highlighting that water content and leaf structural changes appear to be the primary distinguishing factors between the two groups.

- PARAFAC analysis

Before delving into this section, it is important to mention that a Principal Component Analysis (PCA) was initially conducted on the spectroscopic results for each day. The objective was to identify two distinct clusters in the score plot, which would effectively separate the two groups. Additionally, the loading plot was examined to identify the most significant bands contributing to group separation. While this approach yielded successful results for some days, it was not consistently effective across all days. Furthermore, the information obtained from the PCA analysis did not provide substantial clarity or offer substantially distinct insights compared to those derived from Figure 3. Consequently, an alternative feature extraction technique was employed. Exploiting the fact that the data are organized in the form of a three-dimensional array (rows = samples) × (columns = wavelengths) × (sheets = days), a method called PARAFAC (Parallel Factor Analysis) was adopted [47]. PARAFAC facilitates a trilinear decomposition directly on the three dimensions of the data, providing a comprehensive overview of the entire process across the five days rather than isolated analyses for each individual day. Furthermore, each dimension undergoes compression, similar to PCA. For instance, in the wavelength dimension, more than 2000 variables were condensed to just three factors, effectively explaining the majority of data variability. Ultimately, each dimension is characterized by a reduced number of factors through the application of the PARAFAC technique. This reduction in dimensionality allows for a more concise representation of the data while still capturing the essential information and variability present in each dimension. After applying a Savitzky–Golay filter to the MSC-transformed data, the following results were obtained. The filter had a width of 155 points, approximately equivalent to 30 nm, and a polynomial order of 2 with a derivative order of 1. This filtering technique emphasized the shape of the spectra, enabling improved discrimination between the groups. However, as a trade-off, the clarity regarding the specific wavelengths' contributions was reduced. The adoption of a large filter width was necessary to effectively remove noise from the data. The model presented in this study was ultimately reduced to two factors. The primary criterion for determining the number of factors was the core consistency check, which was performed using the loadings obtained from the PARAFAC model. When three factors were considered, the core consistency check did not pass, leading to the decision to retain only two components. While including more factors could potentially account for additional variability in the data, it would primarily capture noise. The first two components explain 44% of the total data variability on the adaxial side and 43% on the abaxial side. Although there is still unexplained variability, these two components are sufficient to capture the differences between the two groups.

Figure 6 displays the PARAFAC results obtained from the adaxial side data, and Figure 7 shows the corresponding results for the abaxial side.
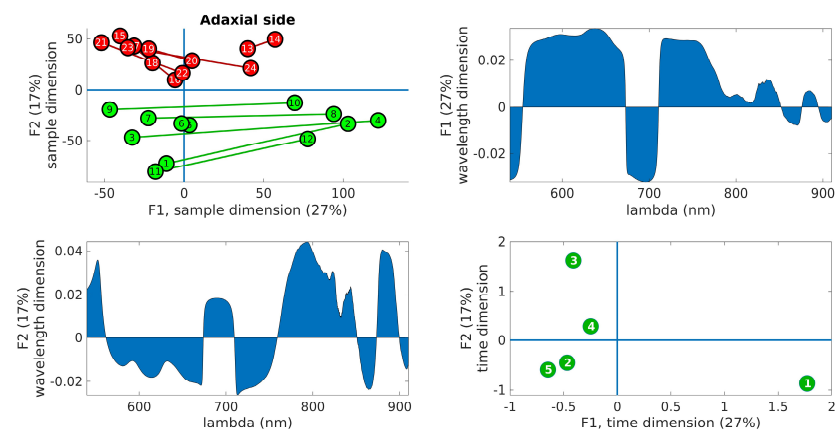

Figure 6. PARAFAC results obtained from the adaxial side data. (**Upper right**): plot of the samples' scores in the first two components. Control leaves are depicted in green, while inoculated leaves are shown in red. The lines join the leaves from the same tree. (**Upper left**): wavelength loadings in the first component. (**Lower left**): wavelength loadings in the second component. (**Lower right**): plot of the loadings associated with the third dimension (time) in the first two components. The digits represent the sample number (1–12, control, 13–24, inoculated).
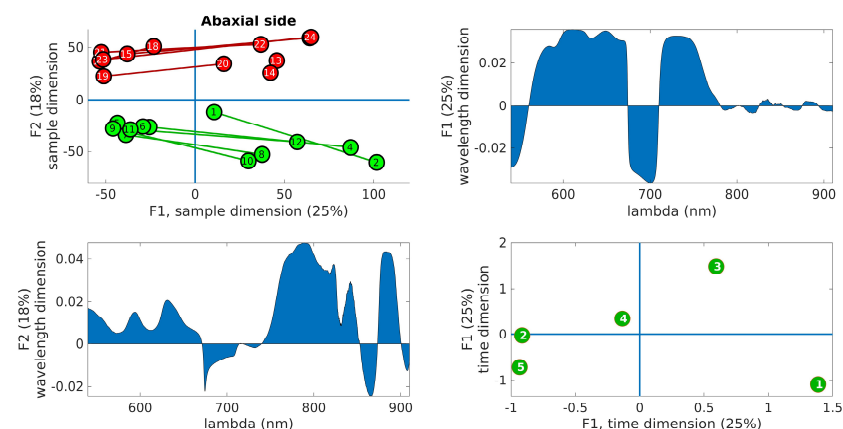

Figure 7. PARAFAC results obtained from the abaxial side data. (**Upper right**): plot of the samples' scores in the first two components. Control leaves are depicted in green, while inoculated leaves are shown in red. The lines join the leaves from the same tree. (**Upper left**): wavelength loadings in the first component. (**Lower left**): wavelength loadings in the second component. (**Lower right**): plot of the loadings associated with the third dimension (time) in the first two components. The digits represent the sample number (1–12, control, 13–24, inoculated).

In the upper right panel, the scores of the samples are plotted in the first two components, where control leaves are represented by green markers and inoculated leaves by red markers. The upper left panel shows the wavelength loadings in the first component, while the lower left panel illustrates the wavelength loadings in the second component. Finally, the lower right panel exhibits the loadings associated with the third dimension (time) in the first two components. The upper right plots in these figures reveal the most notable observation. A distinct separation between the two groups is evident along the second factor. Generally, the control samples exhibit values of F2 < 0, while the inoculated samples show values of F2 > 0, a trend that holds true for both adaxial and abaxial sides. Additionally, an interesting observation is that the first factor, F1, appears to capture variations within the same tree, while the second factor, F2, captures variations between the

trees. This distinction arises because the segments connecting each pair of leaves from the same tree align predominantly with the F1 axis, indicating that tree-related variations are primarily associated with variations in F1. This pattern is more pronounced in the control leaves compared to the inoculated leaves, particularly on the adaxial side. The reduced parallelism observed in the inoculated group suggests internal changes resulting from the infection. The area plots (upper right and lower left) illustrate the loadings across the wavelength dimension. F1, which corresponds to intra-tree variations, exhibits significant contributions primarily below 750 nm. On the other hand, F2, associated with inter-tree variations, demonstrates substantial contributions primarily above 750 nm. Consequently, intra-variations are predominantly linked to changes in pigments, while inter-variations (which enable group differentiation) are primarily associated with water content and leaf structural changes. These findings align with the previous conclusions drawn from the direct spectral analysis as well as the examination of vegetation indices, reinforcing the overall consistency of the results. The final subplot in the lower left showcases the loadings along the time dimension, which corresponds to the order of the measurement days. Its interpretation follows the previously assigned meanings of F1 and F2. For instance, the first and last days exhibit the greatest separation in terms of the first factor, indicating that the leaves from these days are the most dissimilar in terms of pigment content. This can be attributed to the natural aging process of the leaves. Conversely, in terms of water and structural changes (F2), the first and fifth days appear to converge towards a similar state by the end of the experiment. This observation is consistent with the spectral analysis in Figure 3, where the first and fifth rows exhibit relatively similar patterns, with fewer red bands compared to the other three days. However, caution is required when interpreting other observations due to the derivative spectra used in the analysis performed by PARAFAC. For instance, in both Figures 6 and 7, it is the third day that appears to be the furthest from the rest in terms of F2, suggesting it is the day with the most significant differences between the two groups. On the contrary, Figures 3 and 5 indicate that the fourth day exhibits more discriminative bands. The resolution to this apparent contradiction lies in recognizing that PARAFAC results are based on derivative data, and it is plausible that the rate of changes is higher on the third day, leading to a more pronounced separation along the F2 axis.

3.2. Leaf Gas Exchange Measurements

Globally, both plant groups exhibited similar values for the net photosynthetic rate (P_N), transpiration rate (Tr), stomatal conductance (g_s), intercellular CO_2 concentration (C_i), and water-use efficiency (WUE) (Table 3). Indeed, no statistically significant differences ($p < 0.05$) were found between the control and the inoculated plants at any of the sampling dates.

Table 3. Leaf gas exchange in control and inoculated plants determined under environmental conditions. The temporal global mean (5 samplings) and standard deviation of 12 independent replicates (2 leaves per plant; 6 control/inoculated plants) are shown in the table.

Physiological Parameters *	Control Samples (N = 6 × 2 × 5)		Inoculated Samples (N = 6 × 2 × 5)	
	Mean	**Std. Deviation**	**Mean**	**Std. Deviation**
P_N (μmol CO_2 m^{-2}s^{-1})	7.76	0.65	9.41	0.47
g_s (μmol m^{-2}s^{-1})	0.1008	0.0094	0.0895	0.0081
C_i (μmol CO_2 mol^{-1})	240.59	14.62	227.24	14.05
Tr (mmol H_2O m^{-2}s^{-1})	2.8692	0.3566	2.7638	0.3180
WUE (μmol CO_2/mmol H_2O)	3.62	0.30	3.63	0.27
Environmental conditions **	Control Samples		Inoculated Samples	
Tair (°C)	27.83	0.37	30.11	0.34

Physiological Parameters *	Control Samples (N = 6 × 2 × 5)		Inoculated Samples (N = 6 × 2 × 5)	
	Mean	Std. Deviation	Mean	Std. Deviation
PARo ($\mu E\ m^{-2}s^{-1}$)	1485.917	117.3678	1512.050	117.2944
RH (%)	35.24	1.78	30.39	1.66
VPDL (kPa)	2.60	0.13	3.19	0.14

* Net photosynthetic rate (P_N); transpiration rate (Tr); stomatal conductance (g_s); intercellular CO_2 concentration (C_i); and water-use efficiency (WUE). ** Tair: air temperature; PARo: external photosynthetically active radiation; RH: air relative humidity; and VPDL: leaf-to-air water vapor pressure deficit.

3.3. Variation Pattern of Physiological Parameters and Biochemical Parameters

The pigment content (chlorophyll-a (chl *a*); chlorophyll-b (chl *b*); and total carotenoids (t*car*)) was calculated according to Lichtenthaler (1987) [44,45], and the results obtained on average for the control and for the inoculated plants are shown in Table 4.

Table 4. Results obtained on average for chlorophyll-a (Chl *a*), chlorophyll-b (Chl *b*), and total carotenoids (t*car*) in the inoculated and control plants. The mean and standard deviation are shown, as well as pigment ratios or combinations.

Pigments	Control Samples		Inoculated Samples	
	Mean	Std. Deviation	Mean	Std. Deviation
Chl *a* (mg/cm^2)	0.0454	0.0131	0.0435	0.0047
Chl *b* (mg/cm^2)	0.0082	0.0033	0.0091	0.0014
t*car* (mg/cm^2)	0.0120	0.0033	0.0122	0.0018
Pigment ratios/combinations	Control samples		Inoculated samples	
Chl *a* + *b* (mg/cm^2)	0.0536		0.0526	
Chl *a/b*	5.5		4.8	
Chl *a* + *b*/t*car*	4.5		4.3	

In our sample, chlorophyll-a content was lower in inoculated plants than in control plants, with no statistically significant differences. For the other pigments also, no values were found that differed significantly between the inoculated and non-inoculated samples.

Although there were no statistically significant differences between the two plant samples, a behavior trend was observed for chlorophylls similar to that observed by Daoudi et al. [48] in trials with cork oaks from humid and semi-arid regions subjected to water stress.

Soluble sugar concentration expressed as mg per cm^2 of leaf area was slightly higher in inoculated plants for fructose and glucose, with no statistically significant differences between control and inoculated plants (Table 5).

The plants inoculated with *P. cinnamomi* did not accumulate soluble sugars in values significantly different from control plants. The results obtained for the leaf proteome in this same assay stated that "the dynamics of proteins associated with sugar metabolism and sugar signaling reveals a metabolic tendency *in favour* of energy production and reducing power as opposed to the accumulation of sucrose and carbohydrates as reserve substances" [30].

Table 5. Results obtained on average for glucose, fructose, saccharose, and starch in the inoculated and control plants. The mean and standard deviation are shown.

Sugars	Control Samples		Inoculated Samples	
	Mean	**Std. Deviation**	**Mean**	**Std. Deviation**
Glucose (mg/cm^2)	0.0265	0.0080	0.0299	0.0152
Fructose (mg/cm^2)	0.0135	0.0074	0.0206	0.0191
Sacarose (mg/cm^2)	0.3619	0.1010	0.3571	0.0623
Starch (mg/cm^2)	0.1198	0.0558	0.1341	0.0862

4. Conclusions

During a plant–pathogen interaction, the homeostatic state of the participants varies over time. The immune response of plants to the oomycete differs from plant to plant, and the plasticity of spectroscopic profiles in inoculated plants should exceed that of control plants.

The provided description of the observed spectral changes between 63 and 255 DAI is consistent with the measurements. Here is a summary of the key points:

1. At 63 DAI, slight changes in the mesophyll, primarily influenced by water content, are observed. These subtle differences are predominantly detected at the red edge around 750 nm;

2. By 78 and 91 DAI, clear differentiation between the control and inoculated groups becomes apparent, particularly concerning the water bands. The variations in water content contribute significantly to the distinguishable patterns observed;

3. At 126 DAI, the impact of water content changes extends throughout the entire mesophyll structure. This is evidenced by a broad range in the NIR region where reflectance differences are observed;

4. At 248 DAI, following the summer season, the pigments' content remains similar between the control and inoculated groups. However, distinct alterations in the leaf structure become evident, leading to the following observations:

    (a) The spongy mesophyll of the control group undergoes changes that render it structurally similar to that of the inoculated group;

    (b) Differential changes occur in the upper epidermal layer and/or the palisade mesophyll between the control and inoculated groups, resulting in differentiated responses in the visible range.

5. Several vegetation indices exhibit the capability to detect the infection, particularly those related to water content, such as WI (100% success rate) and WBI (80% success rate). Additionally, O1 (or WDVI) achieves a 70% success rate, which may indicate sensitivity to structural changes in the leaves caused by the infection. Interestingly, the widely used NDVI parameter proves to be almost ineffective in detecting the infection, with only a 10% success rate. This emphasizes the importance of considering specific vegetation indices tailored to the target application, as different indices capture different aspects of plant health and physiological changes;

6. The PARAFAC analysis on derivative spectra provided further confirmation of the conclusions derived from the direct spectral analysis and the vegetation indices. It revealed two factors, F1 and F2, which represent different directions of variation in the data. F1 captures the natural physiological variations within the leaves and is primarily influenced by changes in pigment bands in the visible spectrum. On the other hand, F2 is associated with the differences between the control and inoculated plants and is predominantly determined by variations in water content and leaf structural changes, as reflected in the NIR plateau region of the spectra. These findings align with the previous observations and highlight the distinct contributions

of pigments and water/structural changes in discriminating between the control and inoculated plants.

Overall, this description aligns well with the measured data, providing a comprehensive understanding of the observed changes over the course of time.

The results of our study, showing differences in the spectra between control and *P. cinnamomi*-inoculated cork oak plants, are promising. However, it is important to exercise caution in interpreting these findings due to the relatively small number of samples used in the statistical analysis. Further research with a larger sample size is warranted to strengthen the robustness of these observations.

The results of spectroscopy confirm the data from the analysis of the leaf proteome carried out on the same plants [30]. It is confirmed that it is possible to differentiate cork oaks inoculated by *P. cinnamomi* from non-inoculated ones, even when the plants are asymptomatic, by the analysis of proteins present in the leaves and by spectroscopic methods.

Institutional Review Board Statement: Not applicable.

Informed Consent Statement: Not applicable.

Data Availability Statement: Not applicable.

Conflicts of Interest: The authors declare no conflict of interest.

References

1. *6.° Inventário Florestal Nacional—IFN6, Relatório Final*; ICNF (Instituto da Conservação da Natureza e das Florestas): Lisboa, Portugal, 2015.
2. Acácio, V.; Dias, F.S.; Catry, F.X.; Bugalho, N.; Moreira, F. Canopy Cover Loss of Mediterranean Oak Woodlands: Long-term Effects of Management and Climate. *Ecosystems* **2021**, *24*, 1775–1791. [CrossRef]
3. Bento, V.A.; Russo, A.; Vieira, I.; Gouveia, C.M. Identification of forest vulnerability to droughts in the Iberian Peninsula. *Theor. Appl. Climatol.* **2023**, *152*, 559–579. [CrossRef]
4. Duque-Lazo, J.; Navarro-Cerrillo, R.M.; van Gils, H.; Groen, T.A. Forecasting oak decline caused by *Phytophthora cinnamomi* in Andalusia: Identification of priority areas for intervention. *For. Ecol. Manag.* **2018**, *417*, 122–136. [CrossRef]
5. Aubard, V.; Paulo, J.A.; Silva, J.M.N. Long-Term Monitoring of Cork and Holm Oak Stands Productivity in Portugal with Landsat Imagery. *Remote Sens.* **2019**, *11*, 525. [CrossRef]
6. Serrano, M.S.; Rios, P.; Gonzalez, M.; Sánchez, M.E. Experimental minimum threshold for *Phytophthora cinnamomi* root disease expression on *Quercus suber*. *Phytopathol. Mediterr.* **2015**, *54*, 461–464. [CrossRef]
7. Moreira, A.C.; Martins, J.M.S. Influence of site factors on the impact of *Phytophthora cinnamomi* in cork oak stands in Portugal. *For. Pathol.* **2005**, *35*, 145–162. [CrossRef]
8. Gómez-Aparicio, L.; Ibáñez, B.; Serrano, M.S.; De Vita, P.; Ávila, J.M.; Pérez-Ramos, I.M.; García, L.V.; Sánchez, M.E.; Marañón, T. Spatial patterns of soil pathogens in declining Mediterranean forests: Implications for tree species regeneration. *New Phytol.* **2012**, *194*, 1014–1024. [CrossRef]
9. Matías, L.; Abdelaziz, M.; Godoy, O.; Gómez-Aparicio, L. Disentangling the climatic and biotic factors driving changes in the dynamics of *Quercus suber* populations across the species' latitudinal range. *Divers. Distrib.* **2019**, *25*, 524–535. [CrossRef]
10. Serrano, M.; Romero, M.A.; Homet, P.; Gómez-Aparicio, L. Climate change impact on the population dynamics of exotic pathogens: The case of the worldwide pathogen *Phytophthora cinnamomi*. *Agric. For. Meteorol.* **2022**, *322*, 109002. [CrossRef]
11. Cardillo, E.; Abad, E.; Meyer, S. Iberian oak decline caused by *Phytophthora cinnamomi*: A spatiotemporal analysis incorporating the effect of host heterogeneities at landscape scale. *For. Pathol.* **2021**, *51*, e12667. [CrossRef]
12. Bauriegel, E.; Giebel, A.; Geyer, M.; Schmidt, U.; Herppich, W.B. Early detection of *Fusarium* infection in wheat using hyperspectral imaging. *Comput. Electron. Agric.* **2011**, *75*, 304–312. [CrossRef]

13. Ustin, S.L.; Jacquemoud, S. How the optical properties of leaves modify the absorption and scattering of energy and enhance leaf functionality. In *Remote Sensing of Plant Biodiversity*; Springer International Publishing: Cham, Switzerland, 2020; pp. 349–384. [CrossRef]

14. Slaton, M.R.; Raymond Hunt, E., Jr.; Smith, W.K. Estimating near-infrared leaf reflectance from leaf structural characteristics. *Am. J. Bot.* **2001**, *88*, 278–284. [CrossRef] [PubMed]

15. Gausman, H.W.; Allen, W.A. Optical parameters of leaves of 30 plant species. *Plant Physiol.* **1993**, *52*, 57–62. [CrossRef] [PubMed]

16. Dawson, T.P.; Curran, P.J. Technical note: A new technique for interpolating the reflectance red edge position. *Int. J. Remote Sens.* **1998**, *19*, 2133–2139. [CrossRef]

17. Franke, J.; Menz, G. Multi-temporal wheat disease detection by multi-spectral remote sensing. *Precis. Agric.* **2007**, *8*, 161–172. [CrossRef]

18. Buitrago, M.F.; Groen, T.A.; Hecker, C.A.; Skidmore, A.K. Spectroscopic determination of leaf traits using infrared spectra. *Int. J. Appl. Earth Obs. Geoinf.* **2018**, *69*, 237–250. [CrossRef]

19. Kuska, M.T.; Brugger, A.; Thomas, S.; Wahabzada, M.; Kersting, K.; Oerke, E.-C.; Steiner, U.; Mahlein, A.-K. Spectral Patterns Reveal Early Resistance Reactions of Barley Against *Blumeria graminis* f. sp. *hordei. Phytopathology* **2017**, *107*, 1388–1398. [CrossRef]

20. Zahir, S.A.D.M.; Omar, A.F.; Jamlos, M.F.; Azmi, M.A.M.; Muncan, J. A review of visible and near-infrared (Vis-NIR) spectroscopy application in plant stress detection. *Sens. Actuator A Phys.* **2022**, *338*, 113468. [CrossRef]

21. Bajwa, S.G.; Rupe, J.C.; Mason, J. Soybean Disease Monitoring with Leaf Reflectance. *Remote Sens.* **2017**, *9*, 127. [CrossRef]

22. Shi, Y.; Huang, W.; Luo, J.; Huang, L.; Zhou, X. Detection and discrimination of pests and diseases in winter wheat based on spectral indices and kernel discriminant analysis. *Comput. Electron. Agric.* **2017**, *141*, 171–180. [CrossRef]

23. Canário, D.; Figueiredo, E.; Franco, J.C.; Guerra, R.M.F.D.N. Detecting early mealybug infestation stages on tomato plants using optical spectroscopy. *Eur. J. Hortic. Sci.* **2017**, *82*, 341–348. [CrossRef]

24. Lu, J.; Ehsani, R.; Shi, Y.; Castro, A.I.; Wang, S. Detection of multi-tomato leaf diseases (late blight, target and bacterial spots) in diferent stages by using a spectral-based sensor. *Sci. Rep.* **2018**, *8*, 2793. [CrossRef]

25. Abdulridha, J.; Ehsani, R.; Castro, A. Detection and Differentiation between Laurel Wilt Disease, *Phytophthora* Disease, and Salinity Damage Using a Hyperspectral Sensing Technique. *Agriculture* **2016**, *6*, 56. [CrossRef]

26. Sankaran, S.; Mishra, A.; Maja, J.M.; Ehsani, R. Visible-near infrared spectroscopy for detection of Huanglongbing in citrus orchards. *Comput. Electron. Agric.* **2011**, *77*, 127–134. [CrossRef]

27. Newby, Z.; Murphy, R.J.; Guest, D.I.; Ramp, D.; Liew, E.C.Y. Detecting symptoms of *Phytophthora cinnamomi* infection in Australian native vegetation using reflectance spectrometry: Complex effects of water stress and species susceptibility. *Australas* **2019**, *48*, 409–424. [CrossRef]

28. Hardoim, P.R.; Guerra, R.; Rosa da Costa, A.M.; Serrano, M.S.; Sánchez, M.E.; Coelho, A.C. Temporal metabolic profiling of the Quercus suber–*Phytophthora cinnamomi* system by middle-infrared spectroscopy. *For. Path.* **2016**, *46*, 122–133. [CrossRef]

29. Afonso, A.M.; Guerra, R.; Cavaco, A.M.; Pinto, P.; Andrade, A.; Duarte, A.; Power, D.M.; Marques, N.T. Identification of asymptomatic plants infected with Citrus tristeza virus from a time series of leaf spectral characteristics. *Comput. Electron. Agric.* **2017**, *141*, 340–350. [CrossRef]

30. Coelho, A.C.; Pires, R.; Schütz, G.; Santa, C.; Manadas, B.; Pinto, P. Disclosing proteins in the leaves of cork oak plants associated with the immune response to *Phytophthora cinnamomi* inoculation in the roots: A long-term proteomics approach. *PLoS ONE* **2021**, *16*, e0245148. [CrossRef]

31. PLS Toolbox 9.0. Eigenvector Research, Inc.: Manson, WA, USA, 2021. Available online: http://www.eigenvector.com (accessed on 10 March 2022).

32. Rouse, J.W.; Haas, R.H.; Schell, J.A.; Deering, D.W. *Monitoring Vegetation Systems in the Great Plains with ERTS*; Third ERTS-1 Symposium NASA, NASA SP-351; NASA: Washington, DC, USA, 1974; pp. 309–317.

33. Gitelson, A.A.; Kaufman, Y.J.; Merzlyak, M.N. Use of a green channel in remote sensing of global vegetation from EOS-MODIS. *Remote Sens Environ.* **1996**, *58*, 289–298. [CrossRef]

34. Peñuelas, J.; Fillela, I.; Biel, C.; Serrano, L.; Savé, R. The Reflectance at the 950-970 Region as an Indicator of Plant Water Status. *Int. J. Remote Sens.* **1993**, *14*, 1887–1905. [CrossRef]

35. Huete, A.R. A soil-adjusted vegetation index (SAVI). *Remote Sens. Environ.* **1998**, *25*, 295–309. [CrossRef]

36. Baret, F.; Guyot, G. Potentials and limits of vegetation indices for LAI and APAR assessment. *Remote Sens. Environ.* **1991**, *35*, 161–173. [CrossRef]

37. Ceccato, P.; Flasse, S.; Tarantola, S.; Jacquemoud, S.; Grégoire, J.M. Detecting vegetation leaf water content using reflectance in the optical domain. *Remote Sens. Environ.* **2001**, *77*, 22–33. [CrossRef]

38. Gamon, J.A.; Surfus, J.S. Assessing leaf pigment content and activity with a reflectometer. *New Phytol.* **1999**, *143*, 105–117. [CrossRef]

39. Zheng, G.; Moskal, L.M. Retrieving leaf area index (LAI) using remote sensing: Theories, methods and sensors. *Sensors* **2009**, *9*, 2719–2745. [CrossRef]

40. Gamon, J.; Peñuelas, J.; Field, C. A narrow-waveband spectral index that tracks diurnal changes in photosynthetic efficiency. *Remote Sens. Environ.* **1992**, *41*, 35–44. [CrossRef]

41. Merton, R. Monitoring community hysteresis using spectral shift analysis and the red-edge vegetation stress index. In Proceedings of the Seventh Annual JPL Airborne Earth Science Workshop, Pasadena, CA, USA, 12–16 January 1998; pp. 12–16.

42. Daughtry, C.S.; Walthall, C.L.; Kim, M.S.; De Colstoun, E.B.; McMurtrey, J.E., III. Estimating corn leaf chlorophyll concentration from leaf and canopy reflectance. *Remote Sens. Environ.* **2000**, *74*, 229–239. [CrossRef]

43. Merzlyak, M.N.; Gitelson, A.A.; Chivkunova, O.B.; Solovchenko, A.E.; Pogosyan, S.I. Application of reflectance spectroscopy for analysis of higher plant pigments. *Russ. J. Plant Physiol.* **2003**, *50*, 704–710. [CrossRef]

44. Lichtenthaler, H.K. Chlorophylls and carotenoids: Pigments of photosynthetic biomembranes. *Meth. Enzymol.* **1987**, *148*, 350–382. [CrossRef]

45. Lichtenthaler, H.K.; Buschmann, C. Chlorophylls and carotenoids: Measurement and characterization by UV-VIS spectroscopy. *Curr. Protoc. Food Anal. Chem.* **2001**, *1* (Suppl. 1), F4.3.1–F4.3.8. [CrossRef]

46. Karabourniotis, G.; Liakopoulos, G.; Bresta, P.; Nikolopoulos, D. The Optical Properties of Leaf Structural Elements and Their Contribution to Photosynthetic Performance and Photoprotection. *Plants* **2021**, *10*, 1455. [CrossRef] [PubMed]

47. Bro, R. PARAFAC. Tutorial and applications. *Chemometr. Intell. Lab. Syst.* **1997**, *38*, 149–171. [CrossRef]

48. Daoudi, H.; Derridj, A.; Hannachi, L.; Mévy, J.P. Comparative drought responses of *quercus suber* seedlings of three algerian provenances under greenhouse conditions. *Rev. D'ecologie (Terre Et Vie)* **2018**, *73*, 57–70. [CrossRef]